Time reversal focusing of high amplitude sound in a reverberation chamber

Matthew L. Willardson, Brian E. Anderson,[a] Sarah M. Young, Michael H. Denison, and Brian D. Patchett

Acoustics Research Group, Department of Physics and Astronomy, Brigham Young University, Provo, Utah 84602, USA

(Received 29 September 2017; revised 11 January 2018; accepted 23 January 2018; published online 6 February 2018)

Time reversal (TR) is a signal processing technique that can be used for intentional sound focusing. While it has been studied in room acoustics, the application of TR to produce a high amplitude focus of sound in a room has not yet been explored. The purpose of this study is to create a virtual source of spherical waves with TR that are of sufficient intensity to study nonlinear acoustic propagation. A parameterization study of deconvolution, one-bit, clipping, and decay compensation TR methods is performed to optimize high amplitude focusing and temporal signal focus quality. Of all TR methods studied, clipping is shown to produce the highest amplitude focal signal. An experiment utilizing eight horn loudspeakers in a reverberation chamber is done with the clipping TR method. A peak focal amplitude of 9.05 kPa (173.1 dB peak re 20 μPa) is achieved. Results from this experiment indicate that this high amplitude focusing is a nonlinear process.
 https://doi.org/10.1121/1.5023351

[HCS] Pages: 696–705

I. INTRODUCTION

Time reversal (TR) is a signal processing technique that may be used to achieve intentional sound focusing from remotely placed sources.[1,2] The TR process includes a forward step and a backward step. During the forward step, an impulse response (or transfer function in the frequency domain) is obtained between a source and a receiver. The impulse response is then reversed in time and additional processing may be applied at this stage. During the backward step, the reversed impulse response is broadcast from the source and a focusing of sound is achieved at the receiver location. TR has been used in biomedical applications such as lithotripsy of kidney stones and of brain tumors.[3–5] Researchers optimized the strength and spatial confinement of focused waves in these applications by exploiting the complicated wave propagation in the body. It has also been used in the nondestructive evaluation of solid media, to locate and characterize cracks within a sample.[6–10] Some of the applications of TR to nondestructive evaluation, such as the time reversed elastic nonlinearity diagnostic,[8] are similar to lithotripsy except that instead of destroying tissue with intense sound the focused waves are used to excite nonlinear signatures of cracks. Additionally, TR was used to create a high amplitude focusing of ultrasound for a noncontact source used for nondestructive evaluation.[11,12]

This paper describes the use of TR processing to create a high amplitude focus of sound in a reverberation chamber. The purpose of these experiments is to create a virtual source of spherical waves that are of sufficient intensity to study nonlinear acoustic propagation. TR focuses waves to a selected location that converge from all directions to produce the focus, and then diverge from that location.[13] The divergence of the waves after TR focusing may be considered a virtual source.[14] To achieve the highest possible amplitude of TR focusing several methods are explored here, including deconvolution (or inverse filtering), one-bit, clipping, and decay compensation. The comparison of these methods has not been shown to date.

While the TR process has also been applied to room acoustics applications, the authors are not aware of a similar study that seeks to maximize the amplitude of the focusing of sound in a room. Yon *et al.* compared the performance of beamforming to TR focusing in a highly reverberant room with communications applications in mind.[15] Candy *et al.* compared the performance of TR receivers to an optimal linear equalization receiver in extracting a transmitted signal propagating in a highly reverberant environment, with the purpose of improving communications in reverberant environments.[16] Ribay *et al.* performed a time-domain, finite-difference simulation of TR in a two-dimensional (2-D) reverberation room model, also for communications applications, in order to determine the relationship between the signal-to-noise ratio and the number of physical sources, N, used in TR.[17] They concluded that the focal amplitude depends on N, the length of the impulse response T (in units of time), and the reverberation time of the room. In another study, Candy *et al.* examined the functionality of wideband communications with TR receivers in a tunnel with many obstructions, echoes, and bends.[18]

This paper presents a parameterization study to optimize the TR processing methods mentioned previously for high amplitude focusing and temporal signal focus quality. The parameterization study shows that clipping is the method that produces the highest amplitude focus. A final measurement is then presented in which a TR experiment is

[a]Electronic mail: bea@byu.edu

performed with eight loudspeaker horn sources in a reverberation chamber. A peak focal amplitude of 9.05 kPa (173.1 dB peak re 20 μPa) is achieved. Results from this test indicate that the waves that collapse at these high amplitudes are sufficiently high amplitudes to observe nonlinear wave propagation effects.

II. TIME REVERSAL METHODS

This section will review the basics of the deconvolution (inverse filtering), one-bit, clipping, and decay compensation methods. Each of these methods alters the impulse response/transfer function in order to achieve improved focal amplitude or focal quality. The standard TR process involves a time reversal of the impulse response, $ir(t)$ to obtain the time reversed impulse response (TRIR), $ir(-t)$. In the standard TR process, the TRIR is broadcast from each source simultaneously to produce a focus. It should be noted here that prior to the broadcast of a TRIR or a modified TRIR, this signal is normalized to maximize the available amplification.

A. Deconvolution

Deconvolution or inverse filtering has previously been used in TR experiments to achieve a higher quality focal signal, typically at the expense of the focal amplitude.[19–22] Tanter *et al.* found that inverse filtering reduces the amplitude of the side lobes in a TR experiment.[19] The inverse filter method has also been shown to improve the retrieval of the Green's function between the source and receiver in a TR experiment, leading to a cleaner focus (in a signal-to-noise ratio sense, see Sec. III B) than one obtained via standard TR.[21]

One purpose of the deconvolution method, as outlined by Anderson *et al.*, is to obtain a delta function like focal signal.[22] Thus the desired signal to broadcast during the backward step of the TR process is the frequency domain inverse of the transfer function obtained in the forward step,

$$g(\omega) = \frac{1}{R(\omega)} = \frac{R^*(\omega)}{|R(\omega)|^2}, \tag{1}$$

where $g(\omega)$ is the deconvolution transfer function used to obtain focusing, $R(\omega)$ is the transfer function between the source and receiver, and * denotes a complex conjugate. To avoid potentially dividing by 0 in Eq. (1), a regularization constant is added to the denominator,

$$g(\omega) = \frac{R^*(\omega)}{|R(\omega)|^2 + \gamma\,\mathrm{mean}\left(|R(\omega)|^2\right)}, \tag{2}$$

where γ is a unitless, regularization parameter that can be optimized to produce the cleanest focal signal. Equations (1) and (2) were given by Anderson *et al.* though similar equations were given in Refs. 19–21. Figures 1(a) and 1(b) provide examples of an impulse response used for standard TR and an example of a signal obtained after deconvolution, respectively (the deconvolution method is applied to the standard impulse response shown in this figure with $\gamma = 0.9$). The value of γ is optimized later in this study (Anderson *et al.* used a value of $\gamma = 0.9$).

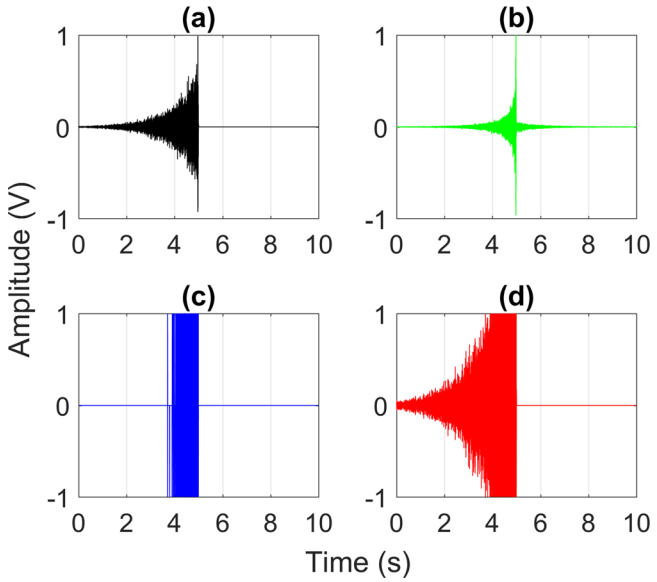

FIG. 1. (Color online) (a) Standard impulse response. (b) Impulse response after deconvolution. (c) Impulse response after one-bit. (d) Impulse response after clipping.

B. One-bit

Derode *et al.* introduced the use of the one-bit method in TR experiments.[23] Their experiments in a water tank achieved an increase of 12 dB in the peak focal amplitude after implementing the one-bit method. The increase in focal amplitude was achieved at the expense of lowering the quality of the time reversal focusing (see Sec. III B).

The one-bit method involves keeping only the phase information of the TRIR signal. For a normalized TRIR, a certain value between 0 and 1 is selected as a threshold and everything above the threshold gets set to +1, and everything below the negative value of the threshold gets set to −1. For the purposes of noise rejection, everything in between the positive threshold and the negative threshold is set to 0. The resulting signal for the backward step only contains values of +1, 0, and −1. Because the phase information is preserved, the one-bit method still focuses energy. An example one-bit processed signal, with a threshold of 0.2, is shown in Fig. 1(c), with this method applied to the standard impulse response shown in this figure. The threshold value is optimized later in this study.

C. Clipping

Clipping was introduced by Heaton *et al.* as a processing method for TR that is very similar to the one-bit method.[24] Like the one-bit method, clipping of the normalized TRIR signal also involves a threshold value. A value between 0 and 1 is selected as a threshold and everything above the threshold gets set to +1, everything below the negative value of the threshold gets set to −1. The difference between the one-bit method and clipping is that for clipping, the signal that lies between the threshold and the negative value of the threshold remains unchanged. An example signal with clipping applied, with a threshold of 0.2, is shown in Fig. 1(d) with the clipping applied to the standard impulse

response shown in this figure. The threshold value is optimized later in this study.

D. Decay compensation

The idea of decay compensation was introduced by Gliozzi *et al.*[25] They sought to compensate for severe attenuation in an impulse response by fitting an exponential decay curve to the impulse response, inverting this decay curve, and then multiplying the square of the inverted decay curve by the impulse response. They argued that this form of decay compensation allowed each reflection arrival in the reversed impulse response to contribute equal amplitude to the TR focus. Each reflected arrival corresponds to an image source and since the energy from each image source must travel the same path that was traveled in the forward step, the same decay rate of energy will occur in the backward step. We will term this form of decay compensation "second order decay compensation" since the inverse of the decay is multiplied by the impulse response twice.

Here we will use what we term "first order decay compensation." Instead of fitting an exponential to the decay in the impulse response, the envelope, $e(t)$, of the normalized TRIR signal is obtained (through a Hilbert transform of the TRIR),

$$e(t) = \sqrt{[ir(-t)]^2 + [\hat{ir}(-t)]^2}, \tag{3}$$

where $\hat{}$ represents a Hilbert transform operator.[26,27] $e(t)$ may be smoothed (for each time sample, the sample and neighboring samples may be averaged). The inverse of the envelope is calculated and multiplied once by the original TRIR signal to obtain the decay compensation signal, $dc(t)$,

$$dc(t) = \frac{1}{e(t)} ir(-t). \tag{4}$$

A threshold value is chosen, such that samples above the threshold (or below the negative value of the threshold) are multiplied by the inverse envelope value while samples below that threshold are unchanged. Figure 2(a) displays $e(t)$ for the $ir(-t)$ given in Fig. 2(a) with a smoothing function. The inverse of $e(t)$ is given in Fig. 2(b). $dc(t)$ is given in Fig. 2(c), with a threshold of 0.05. The threshold value is optimized later in this study.

Thus first order decay compensation multiplies by the inverse decay once while second order decay compensation multiplies by the inverse decay twice. Note that it does not matter whether the inverse decay is multiplied by the forward impulse response or the reversed impulse response so long as the inverse decay information used corresponds to the appropriate forward or backwards direction in time. The focusing in first order decay compensation does not receive equal amplitude contributions from each image source, but the advantage of this technique is that the energy broadcast through the amplifier may be maximized. When one desires to achieve the highest possible focal amplitude then first order decay compensation should be used, since typically the input signals for the backward step are normalized prior to broadcasting them to maximize the available amplifier gain. The use of the envelope of the impulse response also maximizes the available amplification, relative to just using an exponential decay curve, since fluctuations in the impulse response are smoothed out with the envelope approach. In second order decay compensation the late arrivals (which have a lower signal-to-noise ratio) are the highest amplitude portions of the signal broadcast in the backward step, and therefore the earlier reflected arrivals and direct sound are therefore the lower amplitude portions of the signal broadcast in the backward step.

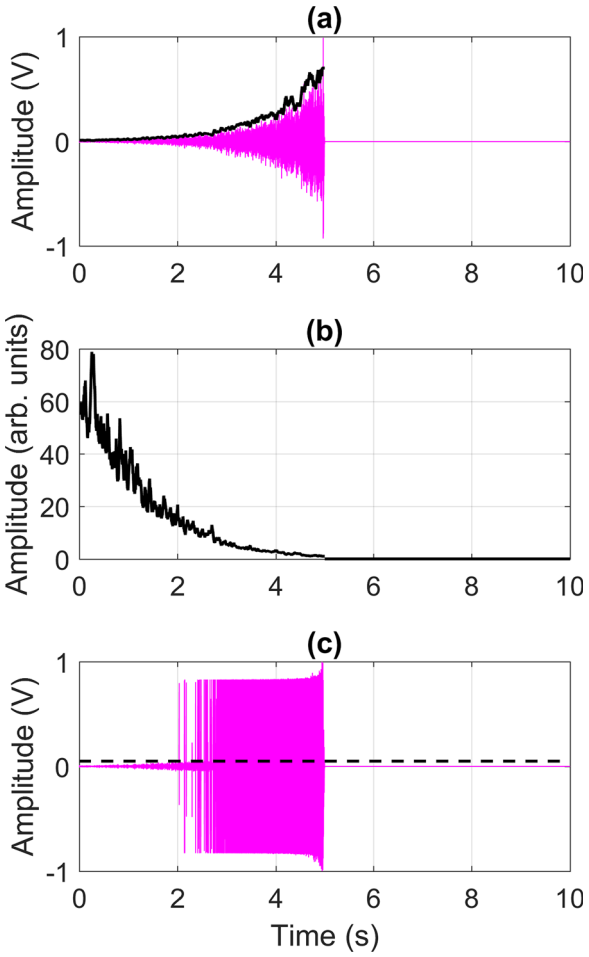

FIG. 2. (Color online) (a) Envelope (black) of the impulse response signal (magenta). (b) Inverse of the envelope in (a). (c) Impulse response after applying decay compensation with the threshold value (dashed black line).

III. FOCAL SIGNAL OPTIMIZATION

This section describes parameterization experiments that are conducted in a reverberation chamber. The TR methods described in Sec. II are each optimized. The length and frequency content of the TRIR are also optimized.

A. Experimental setup

The focal signal optimization tests are performed in a large reverberation chamber (204 m^3) on the Brigham Young University campus. This room is chosen because the hard wall reflections, and therefore long reverberation time,

contribute to a high amplitude focus as shown by Ribay *et al.*[17] The measured reverberation time for the room was found to be 6.89 s and the Schroeder frequency of the room was determined to be 385 Hz.[27] All experiments are performed at frequencies above the Schroeder frequency to ensure a diffuse sound field in the chamber.

The experiments presented in this section employ a single Mackie HR824MK2 loudspeaker as the source and a 1.27 cm (1/2 in.), 46AQ GRAS random incidence microphone with a 53.03 mV/Pa sensitivity as the receiver. A random incidence microphone is chosen for the expected diffuse field in the chamber. Source signals are generated within MATLAB and broadcast from the headphone output on a Dell Latitude E4300 laptop. Data are acquired with a National Instruments PXI-4462 card, housed in a National Instruments 1042 PXI Chassis, with a 204.8 kHz sampling frequency and 24-bit resolution and a LabView program. A photograph of the experimental setup in the room is shown in Fig. 3.

Anderson *et al.* have shown that in rooms, pointing a source directly away from a receiver in a TR experiment yields the highest focal amplitude.[28] Thus the loudspeaker's face is pointed 180° away from the microphone. The loudspeaker's position in the room is 1.54 m from the west wall, 1.85 m from the south wall, and 1.5 m off the ground since room acoustics standards suggest staying at least 1.5 m from any wall to best ensure a diffuse field.[29] Similarly the microphone is placed at least 1.5 m from any wall and is located 1.65 m from the north wall, 1.59 m from the east wall, and 1.61 m off the ground. The distance between the speaker and the microphone is 3.18 m.

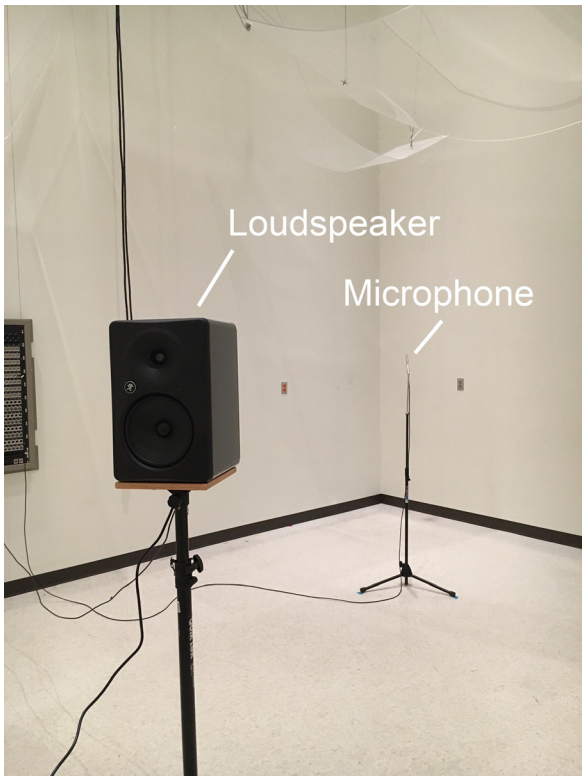

FIG. 3. (Color online) Photograph of the setup used in the optimization experiments in the reverberation chamber.

The source signal, $s(t)$, in the forward step is a logarithmic chirp signal. The pressure response, $r(t)$, is recorded at the microphone. The recording time is set for 10 s to be long enough to exceed the reverberation time. A cross-correlation between $s(t)$ and $r(t)$ is used to estimate the impulse response, $ir(t)$.[28] Depending on the particular experiment, additional processing to implement deconvolution, one-bit, etc. is then applied at this stage to the normalized $ir(t)$. The TRIR was then broadcast from the loudspeaker to produce a focus at the microphone location.

B. Optimization metrics

The peak amplitude and temporal quality are two metrics used here to characterize the focal signal. Peak amplitude, A_P, is a measure of the maximum pressure magnitude (in Pa) achieved in the focal signal. Temporal quality, defined by Heaton *et al.*, compares the squared peak focal amplitude to the average squared pressure present in the signal.[24] Because these experiments involve discrete time signals, the following adapted equation is used to calculate the temporal quality,

$$\xi_T = \sqrt{\frac{[A_P]^2}{\frac{T}{M}\sum_{m=0}^{M}\left[A(x_0,y_0,z_0,m)\right]^2}}, \tag{5}$$

where M is the length of the signal in samples, and $A(x_0,y_0,z_0,m)$ is the amplitude of the mth sample at the microphone focal position (x_0,y_0,z_0). ξ_T is a unitless metric that, with the square root, effectively gives a ratio of peak amplitude to the average pressure magnitude throughout the signal. A delta function signal would have $\xi_T = \sqrt{M}$, a sine wave signal would have $\xi_T = \sqrt{2}$, and a random noise signal would have $\xi_T = \sqrt{3}$.

C. Results of optimization experiments

A total of six sets of optimization experiments are conducted to optimize the TRIR processing: source bandwidth, impulse response length, deconvolution, one-bit, clipping, and decay compensation.

The source bandwidth is varied to determine the bandwidth of the chirp signal that will maximize A_P for standard TR. Thirty-three different bandwidths are tested ranging from 500 Hz to 16 kHz. Frequencies below 500 Hz are not examined due to the Schroeder frequency limit of 385 Hz. The reverberation time in rooms is typically smaller for high frequencies than for low frequencies, thus higher frequency content may not contribute much to TR focusing. The only variable changed in this experiment is the bandwidth of the initial chirp signal, $s(t)$. The first experiment is done over a bandwidth of 7–8 kHz, and the subsequent experiments include more frequency content until a bandwidth of 500 Hz to 16 kHz is reached. The experiments show that adding higher frequency content generally improves ξ_T of the focal signal, while adding lower frequency content degrades ξ_T. However, it is also found that adding lower frequency content does more to boost A_P of the resulting focal signal. This

is likely partly due to the fact that at higher frequencies the absorption is higher and therefore the reverberation would be less significant resulting in lower amplitude image sources in the backward step. The band from 500 to 9500 Hz produced the highest A_P of 17.2 Pa and a ξ_T of 93.3. The rest of the sets of optimization experiments are performed with the optimal 500–9500 Hz band.

The length of the impulse response using standard TR is varied to determine the minimum length of the impulse response needed before A_P is maximized. A nearly 5 s long TRIR is obtained and prior to the broadcast of the TRIR from the loudspeaker, the length of the TRIR was changed. A total of 7 different TRIR lengths were tested, ranging from 0.5 s to the full TRIR length of 4.97 s. The results in Fig. 4 show that shortest length to achieve maximal A_P is around 2.0 s. The minimum length needed in a given room likely depends on the reverberation time in that room. These results confirm those found by Ribay *et al.*, that the length of the impulse response affects A_P.[17]

The experiments optimizing deconvolution are done by obtaining a TRIR and then changing the γ parameter in the deconvolution processing [see Eq. (2)] before broadcasting the modified TRIR from the loudspeaker. One-hundred, logarithmically spaced γ values are tested, ranging from 10^{-6} to 10^{3}. The modified TRIR signal is then broadcast from the loudspeaker and a focal signal is recorded at the microphone for each of the 100 γ values. The results of the deconvolution experiments are shown in Fig. 5. As γ approaches infinity, the deconvolution processing becomes equivalent to standard TR since the magnitude squared term in the denominator of Eq. (2) is small compared to the very large γ term. The modified TRIR is then normalized and Eq. (2) becomes just a standard TRIR. A γ value of zero results in an amplification of noise and therefore a low ξ_T. As described earlier in this section in the literature, deconvolution produces signals with higher ξ_T (ξ_T is related to the signal-to-noise ratio used in the literature) at the expense of a reduction in A_P.

Since the purpose of using deconvolution is to produce focal signals with higher ξ_T, and no value of γ results in a higher A_P than using standard TR, the optimum γ value of 0.1 is selected. This value differs from the γ value of 0.9

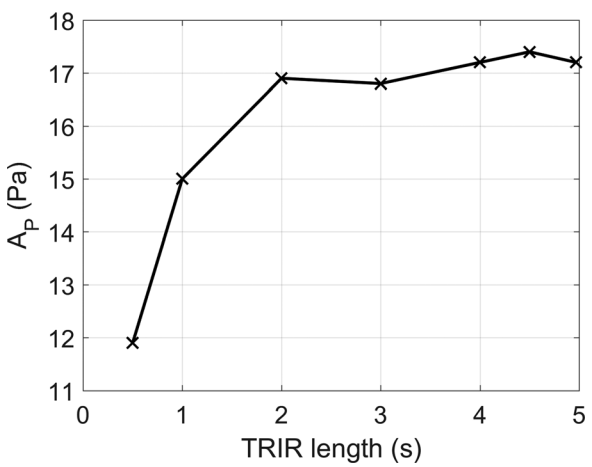

FIG. 4. Peak focal amplitude of a standard time reversal experiment as a function of the length of the impulse response used.

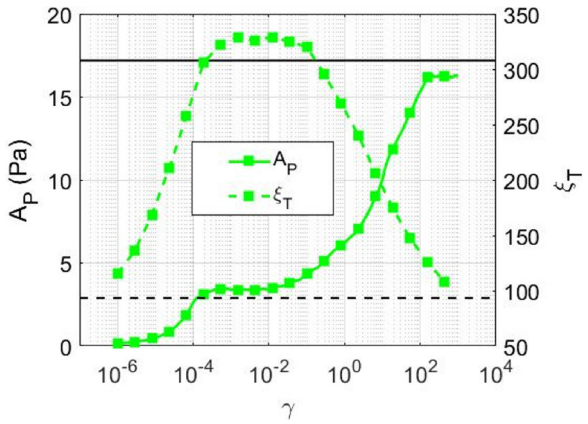

FIG. 5. (Color online) Results of the optimization of deconvolution processing. The focal amplitude, A_P, (solid line) and the temporal quality, ξ_T, (dashed line) are each plotted as a function of the regularization parameter, γ. The solid black line represents the A_P for standard TR, and the dashed black line represents the ξ_T for standard TR.

given by Anderson *et al.*[22] The optimal value for γ may well depend on the available signal-to-noise ratio in the system. Gamma values below 0.1 do not produce focal signals with significantly higher ξ_T, and ξ_T begins to decrease with γ values larger than 0.1. Smaller γ values could be used at the expense of further reductions in A_P. A γ value of 0.1 produced a focal signal with $A_P = 4.4$ Pa and $\xi_T = 320$. Compared to standard TR, the optimal deconvolution focal signal has a ξ_T that is 3.43 times greater, but a A_P that is 3.91 times lower. For the purposes of maximizing A_P, the significant amplitude reduction does not make deconvolution the optimal technique for producing a high amplitude focus.

In the optimization of the one-bit, clipping, and decay compensation signal processing methods, the threshold value is the parameter modified to find the optimum value for high amplitude focusing. Section II described the manner in which the threshold is applied for these methods. For each of these experiments, a TRIR signal is obtained, processed according to the method employed, and then broadcast from the loudspeaker to achieve a focus at the microphone. One-hundred, logarithmically spaced threshold values are tested for each processing method, ranging from 10^{-5} to 1.

The results of the one-bit, clipping, and decay compensation sets of experiments are shown in Figs. 6 and 7. Figure 6 compares A_P for the three methods, and Fig. 7 compares ξ_T for the three methods. These results show that decreasing the threshold value generally creates focal signals with a higher A_P for all three types of signal processing. Also, the increase in A_P is gained generally at the expense of decreasing ξ_T.

Of the three processing methods, clipping produces the highest A_P. This makes sense since more energy is broadcast when clipping is used because the low amplitude samples are not zeroed out as they are in one-bit processing. The optimum clipping threshold value of 0.03 produces a focal signal with $A_P = 110.8$ Pa. This means that with the optimum clipping threshold, the A_P of a standard TR focal signal of 17.2 Pa can be amplified by a factor of 6.44. In terms of dB, clipping processing produces a gain of 16.2 dB. There is a

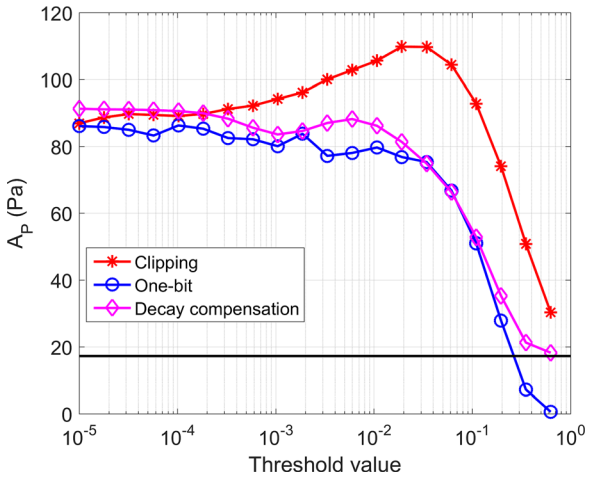

FIG. 6. (Color online) Comparison of the peak focal amplitude, A_P, of the clipping, one-bit, and decay compensation methods over 100 threshold values. The solid black line represents the A_P for standard TR.

decrease in ξ_T, from 93.3 with standard TR down to 72.9 with clipping processing, a 21.9% reduction. The drop in ξ_T is offset by the significant gain in A_P.

The decay compensation method performs better than the one-bit method both in terms of A_P and ξ_T across nearly every threshold value. The optimum threshold value for decay compensation is found to be 0.005. This optimum threshold for decay compensation produced a focal signal with $A_P = 88.5$ Pa and $\xi_T = 61.9$. The A_P of 88.5 Pa is 5.15 times greater than the A_P for standard TR, but it is accompanied with a 33.7% reduction in ξ_T. The optimum threshold value for the one-bit method is found to be 0.02. This optimum threshold for the one-bit method produced a focal signal with $A_P = 78.7$ Pa and $\xi_T = 63.5$. The A_P of the optimal one-bit focal signal is 4.58 times greater than the A_P for standard TR, but ξ_T is 31.9% less than ξ_T achieved with standard TR.

Though not presented here in detail, the clipping, one-bit, and decay compensation methods are applied to the deconvolution modified TRIR signals. The results indicate that both ξ_T (inherited from the deconvolution) and A_P (inherited from the clipping, one-bit, and decay compensation) of the focusing improve compared to standard TR. For clipping with deconvolution, the optimum threshold value is 0.01, slightly lower than the optimum threshold of 0.03 for clipping with standard TR. The optimum threshold for clipping with deconvolution produces a focal signal with $A_P = 43.5$ Pa and $\xi_T = 162.2$. Compared to standard TR, A_P increases by a factor of 2.5 and ξ_T increases by a factor of 1.7. This increase in both A_P and ξ_T shows the robustness of combining deconvolution with clipping techniques to achieve better focusing than standard TR. However the reduction in A_P, relative to when deconvolution is not used, is a drawback to using deconvolution and clipping, for example, to achieve the highest possible focusing amplitude.

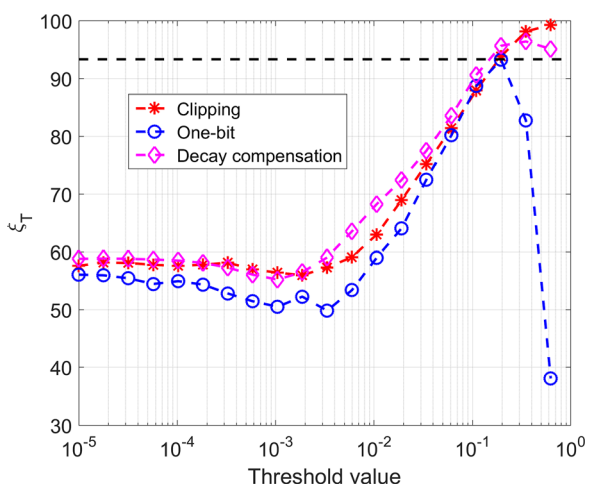

FIG. 7. (Color online) Comparison of the temporal quality, ξ_T, of the clipping, one-bit, and decay compensation methods over 100 threshold values. The dashed black line represents the ξ_T for standard TR.

Before the high amplitude experiments are conducted, a seventh optimization experiment is done to determine the best placement of the sources to achieve the highest possible amplitude for TR focusing. Experiments are conducted with a microphone in the same location as it was in the other optimization experiments (on a stand, 1.61 m off the ground). The loudspeaker is moved to different locations in the room, and a standard TR experiment is done at each location to determine optimum speaker placement for the highest amplitude focus. The results show that the highest amplitude is achieved when the speaker and the microphone are in the same horizontal plane (the primary axis of the loudspeaker is directed in the plane of the microphone), and when the loudspeaker and microphone are placed in corners of the room. These gains due to source and receiver placement in the room are on the order of up to 6 dB gains and likely result from a significant change to the radiation impedance loading (specifically an increase in the radiation resistance) seen by the compression driver horns. When the horns are placed facing the wall they radiate into a smaller open area between the horn opening and the wall as compared to the case when the horn is facing the center of the room.

IV. HIGH AMPLITUDE FOCUSING

Building off the results of Sec. III, a new set of experiments are designed to achieve a high focal amplitude by using the optimal processing of the TRIR, more efficient sound sources, and larger N. The high amplitude focusing measurements are performed in the same reverberation chamber as the optimization experiments. The setup consists of eight BMS 4590 coaxial compression drivers with horns attached to the drivers. One 0.3175 cm (1/8 in.) 40DP GRAS free-field microphone with a 26AC GRAS preamplifier is used for these measurements. Random incidence microphones were unavailable for this size microphone. The microphone has a sensitivity of 0.76 mV/Pa. The microphone has a specified dynamic range upper limit of 175 dB (178 dB peak or 15.9 kPa) for a ± 1 dB precision. A 12AA GRAS microphone power supply is used to power the microphone. The signals presented in this section are the result of using 10 averages.

The signals used for these experiments are created in MATLAB and output via two, 4-channel Spectrum M2i.6022-exp generator cards. The acquisition is done with one, 4-

channel Spectrum M2i.4931-exp digitizer card. A sampling frequency of 50 kHz is used and the digitizer has 16 bit precision. The output from the Spectrum cards is amplified with two, 4-channel Crown CT4150 amplifiers. The eight amplified signals are routed through patch panels via Speakon cables into the reverberation chamber and then to the horn drivers. A panoramic photograph of the setup for the high amplitude focusing experiments is shown in Fig. 8.

Based on the results of the optimization experiments, the drivers are placed close to the corners of the room or close to the adjoining boundary of a wall and the floor. The orientation of each driver is facing nearly 180° away from the microphone. The microphone is placed 3 cm away from a corner in the room in order to achieve the highest possible A_P.

Due to constraints on the upper frequency limit of the mid-range coaxial compression driver, the bandwidth of the initial chirp signal is 500–7500 Hz. This is not a significant issue in terms of amplitude reduction however, because in the earlier optimization experiments the difference in A_P is minimal between the optimal bandwidth of 500–9500 Hz and the bandwidth of 500–7500 Hz. The Crown amplifiers are set to zero attenuation and the output voltage on the Spectrum M2i.6022-exp generator cards is set to 0.6 V peak. The amplifiers provide a 27 dB gain creating an output voltage signal of 8.78 V peak with a 0.392 V peak input signal, which should draw 9.63 W of power in a nominal 8 Ω load. The horns are rated for 150 W of continuous power, thus the amplifier and horns were used well within their linear operating ranges. The clipping TR processing was used throughout this section to create the highest focal amplitude possible within the linear range of the microphone.

In order to observe whether the TR focusing at these amplitudes is a linear or a nonlinear process, four experiments are performed with the clipping method, each with a different input voltage. The input voltages are 0.049 V (Level 1), 0.098 V (Level 2), 0.196 V (Level 3), and 0.392 V (Level 4). Note that each level increase in voltage represents an increase by a factor of 2. For each case the input attenuation knobs are fixed at 0 dB attenuation. If the focusing is a linear process then the lower amplitude focal signals should be identical to the highest amplitude focal signal when scaled up linearly, aside from background noise. The four focal signals obtained with each input voltage level are shown in Fig. 9(a). One can observe the impulsive focusing at the 10.4856 s mark. Figure 9(b) shows the same data with a different time interval to see the amplitudes around the time of peak focusing. The peak compression (positive peak) magnitudes are 0.951, 1.96, 4.10, and 9.05 kPa, respectively, or 153.5, 159.8, 166.2, and 173.1 dB peak, respectively. Note that the differences between successive levels are 6.1, 6.3, 6.4, and 6.9 dB, when a 6.0 dB, representing a pressure doubling, would be expected for a linear system. Thus all recorded amplitudes are within the microphone's specified ±1 dB range.

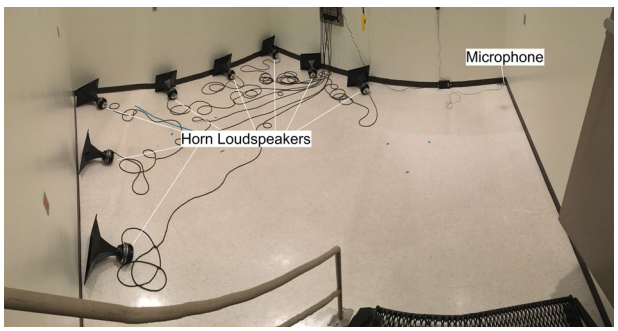

FIG. 8. (Color online) Panoramic photograph of the high amplitude focusing experimental setup in the reverberation chamber.

Linearly scaled versions of these focal signals are shown in Fig. 9(c). Linear scaling is done by multiplying each focal signal by the highest input voltage level, $A_4 = 0.392$ V, and dividing by the corresponding ith input voltage level, $A_i, = 0.049$, 0.098, 0.196, and 0.392 V such that if the focusing were a linear process, all focal signals would match the highest voltage level focal signal. The linearly scaled peak compression magnitudes are 7.61, 7.82, 8.20, and 9.05 kPa, respectively. If the scaled, Level 1 peak compression magnitude is assumed as a reference scaled magnitude then the scaled magnitudes of the compression peaks of the four different focal signals are 1.00, 1.03, 1.08, and 1.19 times the reference scaled magnitude, respectively, meaning that the Level 4 peak magnitude is 19% more the magnitude it should be if it scales linearly. Interestingly, on either side of the peak compression one can observe that the rarefactions nonlinearly decrease in magnitude. This nonlinear increase in the magnitude of the peak compression as the input voltage is increased and the nonlinear decrease in the magnitude of the rarefactions (negative peaks) on either side of the peak compression requires further study. Figure 9(d) shows a segment of the scaled focal signals displayed in Fig. 9(c) at a time before the focal time. This figure shows that the signals scale linearly at these lower amplitudes before the maximal focusing occurs. In fact, all of the focal signals linearly scale before the time of focus, but linear scaling does not hold when the amplitudes rise significantly near the time of focus [the time window shown in Fig. 9(c)] nor does linear scaling hold after the time of focus. A more in depth study of the spatial dependence of this focusing of high amplitude waves is planned for future work. However, because the instantaneous amplitudes of the scaled focal signals linearly scale before the time of focusing, one would expect linear scaling elsewhere in the room before the time of focusing since the energy that arrives at the focal location before the focal time had traveled elsewhere in the room before it arrived there. Therefore it is logical to assume that linear scaling would exist everywhere else in the room before the time of focusing as long as the amplitudes are low in other room locations.

While a more complete study of these nonlinear effects is beyond the scope of this paper, it is interesting to observe changes in the frequency spectra of the focal signals. Figure 10(a) shows scaled sound pressure level spectra for the entire focal signals. These spectra have been smoothed with a 20 ms sliding window to more easily observe changes in the spectra. Only frequency content between 400 Hz and 2 kHz are shown since the majority of the amplitude in these spectra are contained within this band. Note that the Level 1 background noise is approximately at a level of 53 dB. This noise level is highest in the Level 1 spectrum because of the

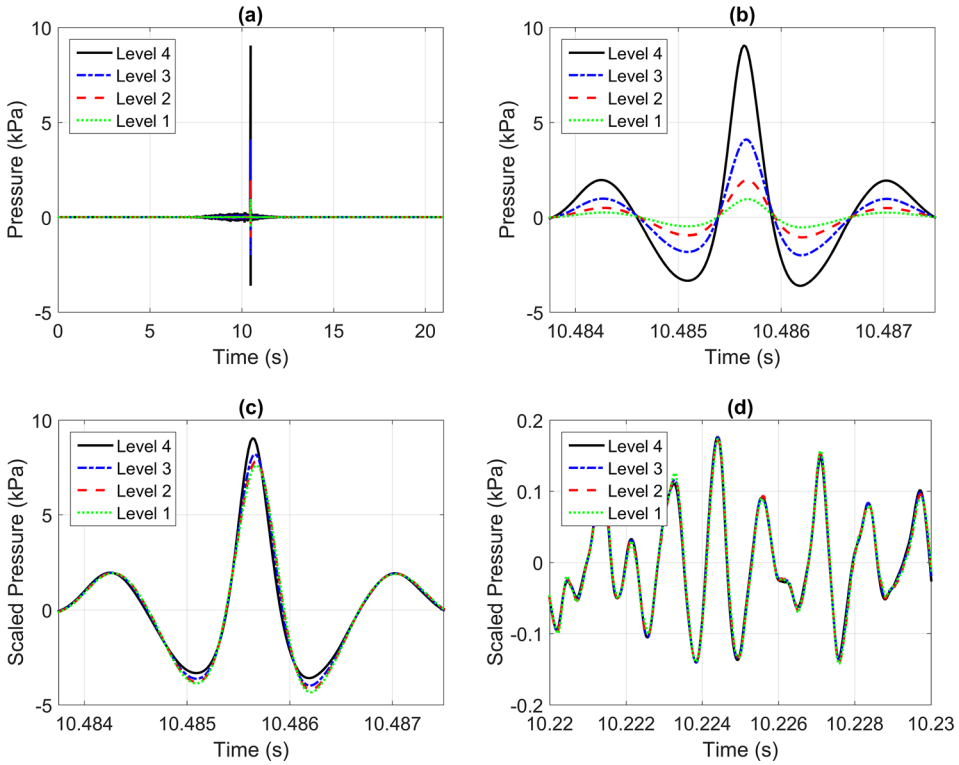

FIG. 9. (Color online) Focal signals obtained from the clipping TR method at high amplitudes. (a) Unscaled focal signals for Levels 1–4. (b) Zoomed in version of (a). (c) Scaled focal signals for Levels 1–4 at a zoomed in time scale. (d) Scaled segment of the focal signals away from the time of peak focusing for Levels 1–4.

linear scaling of the focal signals. In order to more easily see the changes in the spectra with increased input amplitude, the scaled spectra are compared to the Level 1 spectrum by subtracting the Level 1 spectrum from a given scaled spectrum, similar to the procedure proposed by Scalerandi *et al.*[30] These spectral differences are shown in Fig. 10(b). One can observe the decrease in the spectral amplitudes with increased input amplitude between 530 and 1065 Hz by as much as 0.4 dB when comparing the Level 4 spectrum to the Level 1 spectrum. Between 1065 and 2000 Hz there is a noted increase in spectral amplitudes by as much as 7.4 dB when comparing the Level 4 spectrum to the Level 1 spectrum. Note that below 500 Hz it is expected that the signal would drop off because that was the starting frequency of the original chirp signal. The scaled and subtracted spectra should not be reliable below 500 Hz. The low frequency

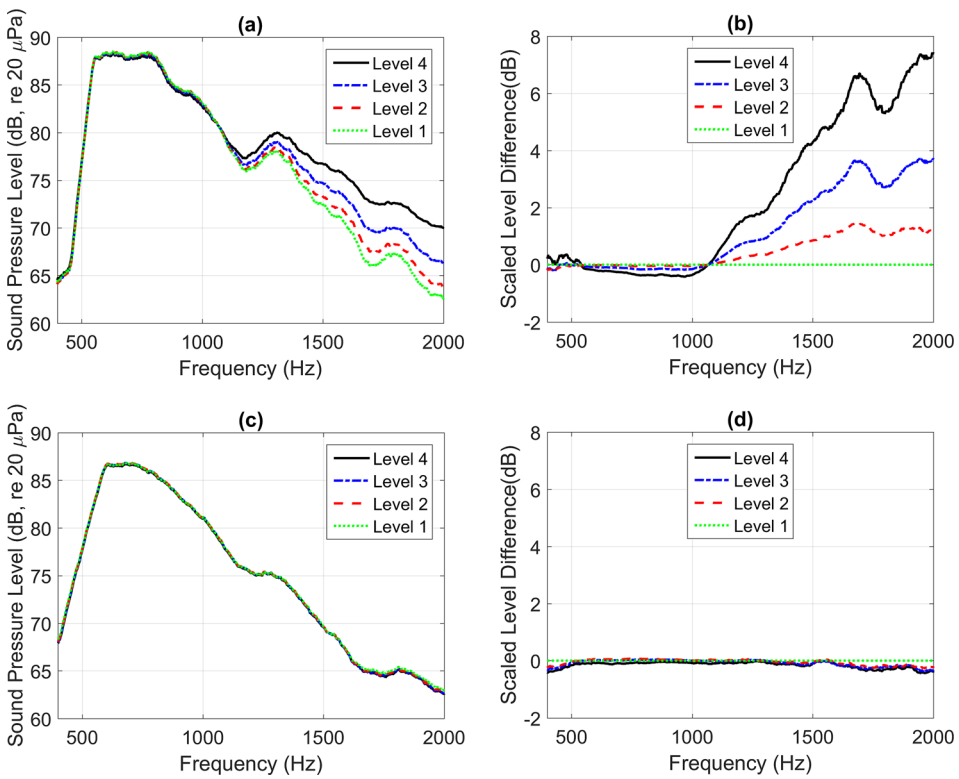

FIG. 10. (Color online) Focal signal spectra obtained from the clipping TR method at high amplitudes. (a) Scaled, focal signal spectra for Levels 1–4 (spectra obtained using the full focal signals). (b) Results of a subtraction of the scaled spectra from Levels 1–4 minus the scaled spectrum of Level 1. (c) Shortened, scaled, focal signal spectra for Levels 1–4 (spectra obtained using the only the portions of the focal signals before the focal time). (d) Results of a subtraction of the shortened, scaled spectra from Levels 1–4 minus the shortened, scaled spectrum of Level 1.

(500–1065 Hz) amplitudes in the higher input amplitude spectra are decreased while the high frequency (1065–2000 Hz) amplitudes in the higher input amplitude spectra are increased. If we now only consider the portion of each focal signal before the focal times, from time zero up until 10.4 s, we can plot their scaled spectra in Fig. 10(c). As before we can then use the Level 1 spectrum as a reference and subtract each spectrum from the Level 1 reference spectrum to obtain Fig. 10(d). Note that the spectra displayed in Fig. 10(c) appear to be identical and indeed in Fig. 10(d), we find a maximum deviation of 0.4 dB between the Level 4 spectrum and the Level 1 spectrum at 2000 Hz where the background noise is likely to blame for the differences in scaled spectra. This shows that linear scaling of the focal signals occurs before the time of focus, but when the amplitudes increase at the time of focus then linear scaling no longer is observed.

To put the focal amplitudes we observe in context of the shock formation distance, we assume a nonlinearity parameter of $\beta = 1.2$. For a peak pressure amplitude of 9 kPa, we obtain an acoustic Mach number of $M = 0.06$. Using the lowest frequency, 500 Hz, for our study we obtain an acoustic wave number of $k = 9\,\mathrm{m}^{-1}$ and using the highest frequency, 2000 Hz, for our study we obtain $k = 37\,\mathrm{m}^{-1}$. The plane wave shock formation distance is known to be $\bar{x} = 1/(\beta M k)$, or in relative terms, $\bar{x}/\lambda = 1/(2\pi\beta M)$. If we assume these expressions are applicable to our results, since a shock formation distance for spherical waves is not well established in the literature, $\bar{x}(500\,\mathrm{Hz}) = 1.4\,\mathrm{m}$, $\bar{x}(2000\,\mathrm{Hz}) = 0.38\,\mathrm{m}$, and $\bar{x}/\lambda = 0.47$. This relative shock formation distance calculation suggests that nonlinear wave steepening effects are expected, despite the limitations of our use of the plane wave shock formation distance. One would not expect that shock waves would be well established for our results. It should be noted that the Mach number used in this analysis is valid at the focus location and thus one would expect a longer shock formation distance as a result since the converging waves are of less amplitude than 9 kPa.

A similar analysis of the results of Montaldo *et al.*[31] would suggest $\bar{x}/\lambda = 24$. Shock waves appear to be well established in their focal signal. For their low amplitude result, an input of 0.25 V was used and a peak focal amplitude of about 0.85 bar was observed. For their high amplitude result, an input amplitude of 17 V was used and a peak focal amplitude of about 45 bar was observed. Linear scaling of the 0.85 bar result would suggest an amplitude of 58 bar. Thus Montaldo *et al.* observed a decrease in the focal amplitude, relative to linear scaling, rather than an increase as we observe in our reverberation chamber results. However, the well formed shocks in the results of Montaldo *et al.* suggest that significant attenuation of the focal amplitude may have happened due to losses at the shocks. Our results did show a tendency to steepen the leading edge of compression peaks and a broadening of rarefaction peaks as was observed to a greater extent by Montaldo *et al.*[31] and by Ganjehi *et al.*[32]

In Provo, Utah the elevation is 1387 m (4551 feet) and the measured temperature on the day of the measurements presented in this section is 21.1 °C. Notably, the measured atmospheric pressure is 85.7 kPa instead of the standard value of 101.3 kPa given at sea level. Thus the peak acoustic compression pressure value of 9.05 kPa above atmospheric pressure is 1.11 times atmospheric pressure in Provo (94.7 atm).

V. CONCLUSION

A parameterization study has been presented, seeking to optimize the peak amplitude, A_P, of TR focusing and the temporal quality, ξ_T, of the TR focal signals for deconvolution, one-bit, clipping, and decay compensation TR methods. First order decay compensation is a variant of a previously proposed method that seeks to amplify later arrivals in an impulse response signal in order to maximize the energy broadcast in the backward step. First order decay compensation performed better than the one-bit method both in terms of focal amplitude, A_P, and temporal quality, ξ_T. The optimal regularization parameter, γ, value was found for the deconvolution method, and optimal threshold values were found for the clipping, one-bit, and decay compensation methods. It has been shown that the clipping method is the impulse response modification method that produces the highest amplitude focus of sound in a reverberation chamber.

With eight horn loudspeaker sources in a reverberation chamber and the optimal clipping threshold, $A_P = 9.05$ kPa (173.1 dB peak) was achieved. Experiments conducted at lower amplitudes and scaled appropriately to the highest amplitude result provide evidence that TR focusing at these high amplitudes is a nonlinear process. Compression magnitudes are nonlinearly increased with higher focusing amplitudes whereas rarefaction magnitudes are nonlinearly decreased with higher focusing amplitudes. A decrease in low frequency energy and an increase in high frequency energy in the spectra of the linearly scaled focal signals, along with linear scaling observed before the time of focusing, suggests that the observed distortions are due to amplitude-dependent wave steepening effects. These experiments will be studied in more detail in future work, including spatial scanning of the focus and creating a louder focus with a microphone that can accurately record higher levels. A theoretical model of nonlinear wave propagation for spherically converging waves of high amplitude might be able to help illustrate and predict these nonlinear effects observed as high amplitude waves collapse to provide a time reversal focus.

ACKNOWLEDGMENTS

This work was made possible through the resources provided by the BYU Department of Physics and Astronomy. The authors want to thank Brent Reichman and Kent Gee for their assistance.

[1]M. Fink, "Time reversed acoustics," Phys. Today **50**(3), 34–40 (1997).
[2]B. E. Anderson, M. Griffa, C. Larmat, T. J. Ulrich, and P. A. Johnson, "Time reversal," Acoust. Today **4**(1), 5–16 (2008).
[3]J.-L. Thomas, F. Wu, and M. Fink, "Time reversal mirror applied to litotripsy," Ultrason. Imaging **18**, 106–121 (1996).

[4]J.-L. Thomas and M. Fink, "Ultrasonic beam focusing through tissue inhomogeneities with a time reversal mirror: Application to transskull therapy," IEEE Trans. Ultrason. Ferroelectr. Freq. Control **43**(6), 1122–1129 (1996).
[5]M. Tanter, J.-L. Thomas, and M. Fink, "Focusing and steering through absorbing and aberating layers: Application to ultrasonic propagation through the skull," J. Acoust. Soc. Am. **103**(5), 2403–2410 (1998).
[6]C. Prada, E. Kerbrat, D. Cassereau, and M. Fink, "Time reversal techniques in ultrasonic nondestructive testing of scattering media," Inverse Probl. **18**, 1761–1773 (2002).
[7]E. Kerbrat, C. Prada, D. Cassereau, and M. Fink, "Ultrasonic nondestructive testing of scattering media using the decomposition of the time reversal operator," IEEE Trans. Ultrason. Ferroelectr. Freq. Control **49**, 1103–1113 (2002).
[8]T. J. Ulrich, P. A. Johnson, and A. Sutin, "Imaging nonlinear scatterers applying the time reversal mirror," J. Acoust. Soc. Am. **119**(3), 1514–1518 (2006).
[9]B. E. Anderson, M. Griffa, T. J. Ulrich, P.-Y. Le Bas, R. A. Guyer, and P. A. Johnson, "Crack localization and characterization in solid media using time reversal techniques," in *44th U. S. Rock Mechanics Symposium and 5th U. S.–Canada Rock Mechanics Symposium*, 27–30 June 2010, Salt Lake City, Utah, document no. 10-154.
[10]B. E. Anderson, L. Pieczonka, M. C. Remillieux, T. J. Ulrich, and P.-Y. Le Bas, "Stress corrosion crack depth investigation using the time reversed elastic nonlinearity diagnostic," J. Acoust. Soc. Am. **141**(1), EL76–EL81 (2017).
[11]P.-Y. Le Bas, T. J. Ulrich, B. E. Anderson, and J. J. Esplin, "A high amplitude, time reversal acoustic non-contact excitation (TRANCE)," J. Acoust. Soc. Am. **134**(1), EL52–EL56 (2013).
[12]P.-Y. Le Bas, M. C. Remillieux, L. Pieczonka, J. A. Ten Cate, B. E. Anderson, and T. J. Ulrich, "Damage imaging in a laminated composite plate using an air-coupled time reversal mirror," Appl. Phys. Lett. **107**, 184102 (2015).
[13]B. E. Anderson, T. J. Ulrich, and P.-Y. Le Bas, "Comparison and visualization of the focusing wave fields of various time reversal techniques in elastic media," J. Acoust. Soc. Am. **134**(6), EL527–EL533 (2013).
[14]M. Scalerandi, A. S. Gliozzi, B. E. Anderson, M. Griffa, P. A. Johnson, and T. J. Ulrich, "Selective source reduction to identify masked sources using time reversal acoustics," J. Phys. D Appl. Phys. **41**, 155504 (2008).
[15]S. Yon, M. Tanter, and M. Fink, "Sound focusing in rooms: The time-reversal approach," J. Acoust. Soc. Am. **113**(3), 1533–1543 (2003).
[16]J. V. Candy, A. W. Meyer, A. J. Poggio, and B. L. Guidry, "Time-reversal processing for an acoustic communications experiment in a highly reverberant environment," J. Acoust. Soc. Am. **115**(4), 1621–1631 (2004).
[17]G. Ribay, J. de Rosny, and M. Fink, "Time reversal of noise sources in a reverberation room," J. Acoust. Soc. Am. **117**(5), 2866–2872 (2005).
[18]J. V. Candy, D. H. Chambers, C. L. Robbins, B. L. Guidry, A. J. Poggio, F. Dowla, and C. A. Hertzog, "Wideband multichannel time-reversal processing for acoustic communications in a tunnel-like structure," J. Acoust. Soc. Am. **120**(2), 838–851 (2006).
[19]M. Tanter, J.-L. Thomas, and M. Fink, "Time reversal and the inverse filter," J. Acoust. Soc. Am. **108**(1), 223–234 (2000).
[20]M. Tanter, J.-F. Aubry, J. Gerber, J.-L. Thomas, and M. Fink, "Optimal focusing by spatio-temporal filter. I. Basic principles," J. Acoust. Soc. Am. **110**(1), 37–47 (2001).
[21]T. Gallot, S. Catheline, P. Roux, and M. Campillo, "A passive inverse filter for Green's function retrieval," J. Acoust. Soc. Am. **131**(1), EL21–EL27 (2012).
[22]B. E. Anderson, J. Douma, T. J. Ulrich, and R. Snieder, "Improving spatio-temporal focusing and source reconstruction through deconvolution," Wave Motion **52**(9), 151–159 (2015).
[23]A. Derode, A. Tourin, and M. Fink, "Ultrasonic pulse compression with one-bit time reversal through multiple scattering," J. Appl. Phys. **85**(9), 6343–6352 (1999).
[24]C. Heaton, B. E. Anderson, and S. M. Young, "Time reversal focusing of elastic waves in plates for an educational demonstration," J. Acoust. Soc. Am. **141**(2), 1084–1092 (2017).
[25]A. S. Gliozzi, M. Scalerandi, and P. Antonaci, "One-channel time-reversal acoustics in highly attenuating media," J. Phys. D: Appl. Phys. **46**, 135502 (2013).
[26]J. Vanderkooy and S. P. Lipschitz, "Uses and abuses of the energy-time curve," J. Audio Eng. Soc. **38**(11), 819–836 (1990), available at http://www.aes.org/e-lib/browse.cfm?elib=6007.
[27]J. J. Esplin, B. E. Anderson, T. W. Leishman, and B. T. Thornock, "The effects of non-cardioid directivity on incidence estimation using the polar energy time curve," J. Acoust. Soc. Am. **130**(4), EL244–EL250 (2011).
[28]B. E. Anderson, M. Clemens, and M. L. Willardson, "The effect of transducer directionality on time reversal focusing," J. Acoust. Soc. Am. **142**(1), EL95–EL101 (2017).
[29]ISO 3741:2010, "Acoustics-Determination of sound power and sound energy levels of noise sources using sound pressure—Precision methods for reverberation test rooms" (International Organization for Standardization, Geneva, Switzerland, 2010).
[30]M. Scalerandi, A. S. Gliozzi, C. L. E. Bruno, D. Masera, and P. Bocca, "A scaling method to enhance detection of a nonlinear elastic response," Appl. Phys. Lett. **92**(10) 101912 (2008).
[31]G. Montaldo, P. Roux, A. Derode, C. Negreira, and M. Fink, "Ultrasound shock wave generator with one-bit time reversal in a dispersive medium, application to lithotripsy," Appl. Phys. Lett. **80**(5), 897–899 (2002).
[32]L. Ganjehi, R. Marchiano, F. Coulourat, and J.-L. Thomas, "Evidence of wave front folding of sonic booms by a laboratory-scale deterministic experiment of shock waves in a heterogeneous medium," J. Acoust. Soc. Am. **124**(1), 57–71 (2008).